

Multiple mixed state variable incremental integration for reconstructing extreme multistability in a novel memristive hyperchaotic jerk system with multiple cubic nonlinearity

Meng-Jiao Wang(王梦蛟) and Lingfang Gu(辜玲芳)
Citation: Chin. Phys. B, 2024, 33 (**2**): 020504. DOI: 10.1088/1674-1056/acddd0
Journal homepage: http://cpb.iphy.ac.cn; http://iopscience.iop.org/cpb

What follows is a list of articles you may be interested in

Characteristic analysis of 5D symmetric Hamiltonian conservative hyperchaotic system with hidden multiple stability

Li-Lian Huang(黄丽莲), Yan-Hao Ma(马衍昊), and Chuang Li(李创)
Chin. Phys. B, 2024, 33 (**1**): 010503. DOI: 10.1088/1674-1056/acf9e7

A novel fractional-order hyperchaotic complex system and its synchronization

Mengxin Jin(金孟鑫), Kehui Sun(孙克辉), and Shaobo He(贺少波)
Chin. Phys. B, 2023, 32 (**6**): 060501. DOI: 10.1088/1674-1056/acc0f6

A color image encryption algorithm based on hyperchaotic map and DNA mutation

Xinyu Gao(高昕瑜), Bo Sun(孙博), Yinghong Cao(曹颖鸿), Santo Banerjee, and Jun Mou(牟俊)
Chin. Phys. B, 2023, 32 (**3**): 030501. DOI: 10.1088/1674-1056/ac8cdf

Lossless embedding: A visually meaningful image encryption algorithm based on hyperchaos and compressive sensing

Xing-Yuan Wang(王兴元), Xiao-Li Wang(王晓丽), Lin Teng(滕琳), Dong-Hua Jiang(蒋东华), and Yongjin Xian(咸永锦)
Chin. Phys. B, 2023, 32 (**2**): 020503. DOI: 10.1088/1674-1056/aca149

Memristor hyperchaos in a generalized Kolmogorov-type system with extreme multistability

Xiaodong Jiao(焦晓东), Mingfeng Yuan(袁明峰), Jin Tao(陶金), Hao Sun(孙昊), Qinglin Sun(孙青林), and Zengqiang Chen(陈增强)
Chin. Phys. B, 2023, 32 (**1**): 010507. DOI: 10.1088/1674-1056/ac5e95

Multiple mixed state variable incremental integration for reconstructing extreme multistability in a novel memristive hyperchaotic jerk system with multiple cubic nonlinearity

Meng-Jiao Wang(王梦蛟)† and Lingfang Gu(辜玲芳)

School of Automation and Electronic Information, Xiangtan University, Xiangtan 411105, *China*

(Received 15 April 2023; revised manuscript received 2 June 2023; accepted manuscript online 13 June 2023)

Memristor-based chaotic systems with infinite equilibria are interesting because they generate extreme multistability. Their initial state-dependent dynamics can be explained in a reduced-dimension model by converting the incremental integration of the state variables into system parameters. However, this approach cannot solve memristive systems in the presence of nonlinear terms other than the memristor term. In addition, the converted state variables may suffer from a degree of divergence. To allow simpler mechanistic analysis and physical implementation of extreme multistability phenomena, this paper uses a multiple mixed state variable incremental integration (MMSVII) method, which successfully reconstructs a four-dimensional hyperchaotic jerk system with multiple cubic nonlinearities except for the memristor term in a three-dimensional model using a clever linear state variable mapping that eliminates the divergence of the state variables. Finally, the simulation circuit of the reduced-dimension system is constructed using Multisim simulation software and the simulation results are consistent with the MATLAB numerical simulation results. The results show that the method of MMSVII proposed in this paper is useful for analyzing extreme multistable systems with multiple higher-order nonlinear terms.

Keywords: extreme multistability, hyperchaotic, jerk system, nonlinearity

PACS: 05.45.–a, 05.45.Pq **DOI:** 10.1088/1674-1056/acddd0

1. Introduction

In recent years, chaotic systems have gradually become a popular issue in nonlinear scientific research due to their complex phenomena in nonlinear systems.[1–10] In general, a system with one positive Lyapunov exponent (LE) is called a chaotic system and a chaotic system with at least two Lyapunov exponents (LEs) greater than zero is called a hyperchaotic system.[11–13] Hyperchaos belongs to a kind of chaos but since hyperchaotic systems have at least two positive LEs, their dynamical behavior folds and expands in more directions, and the dynamic properties of hyperchaotic systems are more complex than those of chaotic systems. Therefore, they have a wider prospect for application.[14,15]

The phenomenon of initially correlated multistability is a unique phenomenon for nonlinear dynamical systems and is essential in the search for potential uses in chaotic engineering applications.[16–18] Multistability is the property of multiple different types of attractors coexisting under the same set of system parameters.[19–23] In other words, when the system parameters are fixed, different initial conditions will induce the system to enter different orbits, resulting in very different attractors.[24,25] When the number of coexisting attractors in the same set of parameters tends to infinity, then the system has extreme multistability.[26] Multistability is an intrinsic property of many nonlinear systems and it allows the system to switch between different states without adjusting the parameters, thus increasing the flexibility of the system. Consequently, multistability has become an important research topic.[22,23] Moreover, due to the complexity of hyperchaotic systems, the discovery of extreme multistable hyperchaotic systems is relatively rare.

Due to the special intrinsic structure relationship of ideal memristors, chaotic systems based on memristors usually exhibit extreme multistability phenomena. They generally have no equilibrium points or have line equilibrium points[27–29] or surface equilibrium points[30,31] related to the initial conditions; therefore, they are difficult to operate stably in the long term. Since memristors are often described as dynamic components in the flux-charge domain, the flux and charge can be used as state variables of the system and modeled in a reduced-order form for memristor circuits, which can effectively simplify the system analysis. With this transformation, the initial values of the primitive system can be represented as parameters of the reduced-order system, and the initial relevant dynamical behavior of the primitive system can be shown in the flux-charge domain. Therefore, the incremental flux-charge analysis method[33,34] can easily be used in the study of relatively complex memristive circuits.

Based on the duality of circuit variables,[35] memristive chaotic circuits made up of linear discrete electronic components can easily be modeled as flux-charge. Since flux and charge are time integrals of voltage and current, the basic principle of flux analysis methods is the incremental integral trans-

†Corresponding author. E-mail: wangmj@xtu.edu.cn

© 2024 Chinese Physical Society and IOP Publishing Ltd

formation of state variables,[31] so memristive systems with normalized state variables can be modeled using the incremental integral transformation for order reduction. However, since the integration of higher-order nonlinear terms is difficult to express explicitly, this method can only deal with memristor systems without complex nonlinear terms other than memristors.[28]

To address both of these issues, a hybrid state variable incremental integration (HSVII) method consisting of incremental integral transformations of state variables and linear transformations has been proposed in Ref. [28]. In this paper, a multiple mixed state variable incremental integration (MMSVII) method is proposed based on the HSVII method to solve amnesiac hyperchaotic jerk systems with multiple distinct cubic nonlinear terms. The validity of the proposed method is demonstrated with a four-dimensional memristive hyperchaotic jerk system with two distinct cubic nonlinearities. This four-dimensional amnestic hyperchaotic jerk system has three line equilibria and a large number of coexisting attractors. As a result, it is not easy to measure stably in a hardware circuit. Using the proposed method, the incremental integral transformation is carried out first, and then the integral of the cubic nonlinear term is represented by the newly introduced state variable. However, the new mapping suffers from a certain degree of divergence in the different state variables. In addition, in combination with the characteristics of the equation, the difference between the 1st and 5th state variables and the sum of the 3rd and 4th state variables are selected as the two new state variables, respectively. Through this method, the divergence problem has been successfully solved and a three-dimensional reduced-dimension system has been constructed, which facilitates the mechanistic analysis and physical measurements of the initial state-dependent dynamics of the primitive system. Numerical simulations and simulation experiments demonstrate that the coexisting attractors of the initial four-dimensional memristive hyperchaotic jerk system varying with the initial state of the memristive can be visualized in the reduced-dimension system.

In this paper, a four-dimensional memristive hyperchaotic jerk system is proposed in Section 2, whose extreme multistability phenomena are revealed numerically by bifurcation diagrams, LEs spectra, and phase diagrams. In Section 3, a dimensionality reduction model of this dimensional memristive jerk hyperchaotic memristive system is constructed based on the HSVII. The mechanism for the generation of the initial correlation dynamics is explored by analyzing the stability of the equilibrium point. Finally, in Section 4, simulation circuit experiments are carried out to verify the theoretical and numerical results.

2. A memristive hyperchaotic jerk system with three linear equilibrium points

2.1. Mathematical models

The American scientist Sprott proposed the jerk system in 2000,[36] which is mathematically modeled as

$$\begin{cases} \dot{x}_1 = x_2, \\ \dot{x}_2 = x_3, \\ \dot{x}_3 = -x_2 - \beta x_3 + f(x_1), \end{cases} \tag{1}$$

where $\beta = 0.45$–0.7, when $f(x_1) = |x_1| - 1$, a single scroll chaotic attractor is produced; when $f(x_1) = \mathrm{sgn}(x_1) - x_1$, a double-scroll chaotic attractor is produced.

The flux-controlled memristor[37] used in this paper is

$$q(\varphi) = \varphi - \frac{1}{3}\varphi^3, \tag{2}$$

where $q(\varphi)$ is a nonlinear function and φ is magnetic flux. The incremental memductance function is

$$W(\varphi) = \frac{\mathrm{d}q(\varphi)}{\mathrm{d}\varphi} = 1 - \varphi^2. \tag{3}$$

To verify the characteristics of the memristor, a bipolar sinusoidal voltage is applied across the memristor. When the frequency F_m is 0.5, 2 and 8 for a fixed amplitude $A_\mathrm{m} = 2$, three "8" shaped hysteresis lines are generated, as shown in Fig. 1(a), and it is found that the flap area of the "8" shaped hysteresis lines shrinks as F_m increases. When the frequency is fixed at $F_\mathrm{m} = 2$ and the amplitude A_m is 1, 2 and 3, three "8" shaped hysteresis lines are generated as shown in Fig. 1(b), and the flap area of the "8" shaped hysteresis lines can be found to expand as A_m increases. In summary, it can be seen that the model satisfies the fingerprint characteristics associated with the memristor.

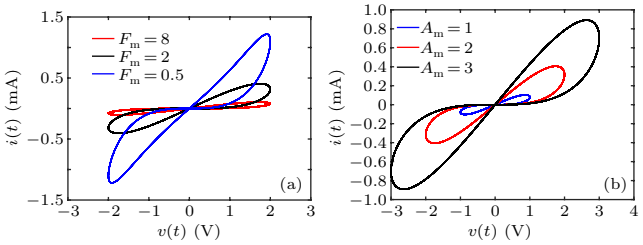


Fig. 1. The relationship between voltage and current for the memristor. (a) $A_\mathrm{m} = 2$, (b) $F_\mathrm{m} = 2$.

By introducing this memristor into the first equation of the original jerk system and adding the fourth equation as the internal equation of state of the memristor, as well as adding some linear and nonlinear terms to the second and third equations, a new four-dimensional jerk memristive chaotic system can be constructed with the following mathematical model:

$$\begin{cases} \dot{x}_1 = (1 - x_4^2)x_2, \\ \dot{x}_2 = x_3 + x_3^3, \\ \dot{x}_3 = x_1 - a x_2 - x_3 - b x_1^3 - x_3^3, \\ \dot{x}_4 = x_2, \end{cases} \tag{4}$$

where parameters a and b are set to 0.68 and 20, respectively, and when the initial conditions of the model are set to $x_2(0) = 10^{-6}$ and $x_1(0) = x_3(0) = x_4(0) = 0$, the memristive jerk system generates a double-scroll chaotic attractor, as shown in Fig. 2.

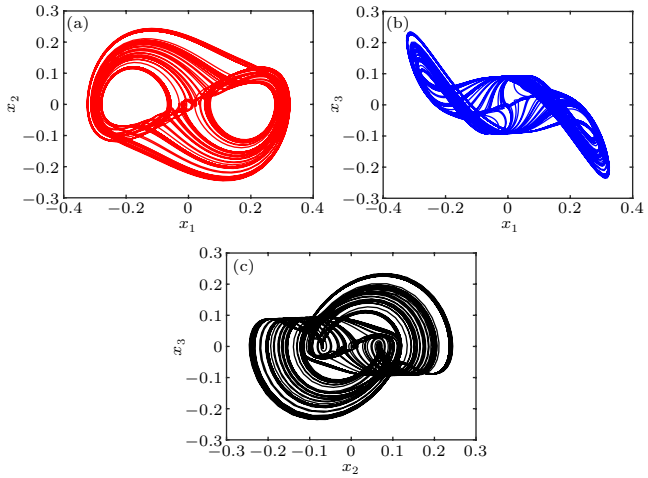


Fig. 2. Phase diagram of the double-scroll chaotic attractor generated by the memristive jerk system when $a = 0.68$, $b = 20$, $x_1(0) = x_3(0) = x_4(0) = 0$. (a) Phase portrait in the x_1–x_2 plane. (b) Phase portrait in the x_1–x_3 plane. (c) Phase portrait in the x_2–x_3 plane.

2.2. System dynamics analysis

2.2.1. LEs spectrum and bifurcation diagram

When the initial condition $x_4(0)$ of the memristor changes, the dynamical behavior of the system will also change greatly. Taking $x_4(0)$ as the change parameter, the bifurcation diagram and the corresponding LEs spectrum are shown in Fig. 3. It is clear that the stable and unstable state regions reflected by each trajectory in the diagram are consistent. The system exhibits complex dynamical behaviors, including periodic attractors, chaotic attractors, proposed periodic attractors, tangential bifurcations, doubly periodic bifurcations, inverse doubly periodic bifurcations, and crises. Observation of the LEs spectrum reveals that in the interval $(-0.2, 0.5)$, as $x_4(0)$ gradually increases, LE1 is always positive, while LE2 is sometimes positive and sometimes negative, thus alternating between hyperchaotic and chaotic states of motion of the system.

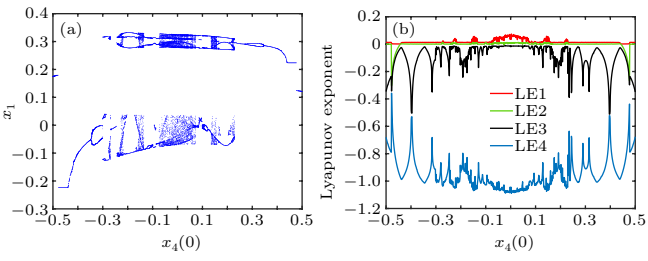


Fig. 3. Bifurcation diagram and LEs spectrum of the memristive jerk system with respect to when $a = 0.68$, $b = 20$, $x_2(0) = 10^{-6}$, $x_1(0) = x_3(0) = 0$. (a) Bifurcation diagram, (b) finite time LEs spectra.

Furthermore, the coexistence bifurcation behavior with respect to parameter a when the initial conditions of the system (1) are set to $(0, 10^{-6}, 0, 0)$ and $(0, -10^{-6}, 0, 0)$, respectively, is shown in Fig. 4. It is not difficult to observe that within the interval $(0.6, 1.2)$, with the increase of the value of parameter a, the system enters period 1 after experiencing chaos, periodic window, and bifurcation, respectively, and then enters short chaotic mode through twice period-doubling bifurcation, and finally reaches the stable point through anti-period-doubling bifurcation and twice period-doubling bifurcation.

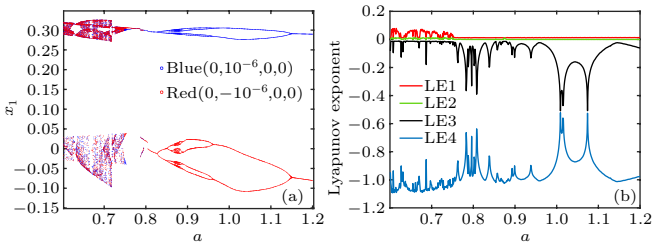


Fig. 4. Bifurcation diagram and LEs spectrum of the memristive jerk system with respect to the parameters when $a = 0.68$, $b = 20$, $x_2(0) = 10^{-6}$, and $x_1(0) = x_3(0) = 0$. (a) Bifurcation diagram, (b) finite time LEs spectra.

2.2.2. Extreme multistability of system

From the bifurcation diagram and the LEs spectrum, it can be seen that the initial conditions have a strong influence on the dynamical behavior of the system and that the system (1) produces various attractors under different initial conditions of the memristor, which means that there is extreme multistability in the system. Some of the typical attractors are shown in Fig. 5. We can also find that tiny changes in the initial conditions of the memristor can lead to significant changes

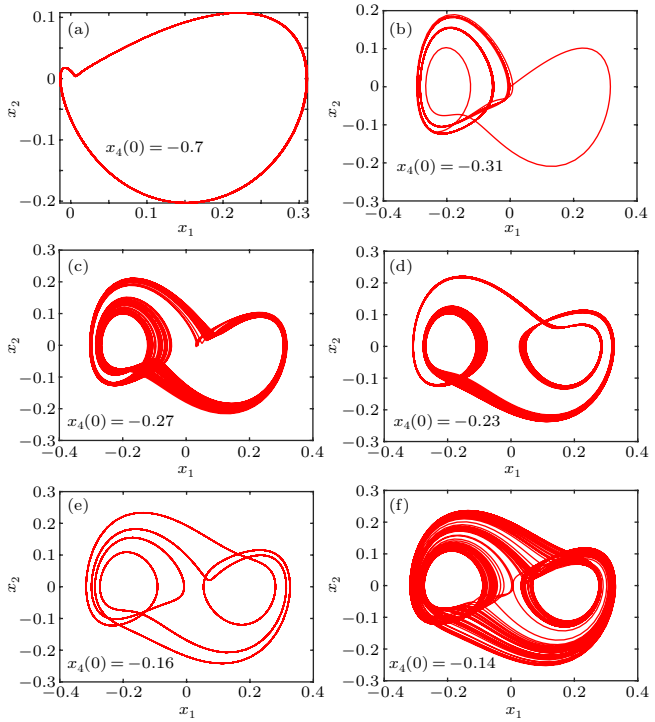


Fig. 5. Memristive chaotic system with various attractors generated under different initial condition. (a) $x_4(0) = -0.7$, (b) $x_4(0) = -0.31$, (c) $x_4(0) = -0.27$, (d) $x_4(0) = -0.23$, (e) $x_4(0) = -0.16$, (f) $x_4(0) = -0.14$.

in the phase diagram of the system, which also reflects the high sensitivity of chaotic systems to initial conditions.

2.2.3. Equilibrium points and stabilities

Zero the right-hand side of system (1), i.e.,

$$\begin{cases} 0 = (1-x_4^2)x_2, \\ 0 = x_3 + x_3^3, \\ 0 = x_1 - ax_2 - x_3 - bx_1^3 - x_3^3, \\ 0 = x_2. \end{cases} \tag{5}$$

For $b \geq 0$, it is clear that the equilibrium points of the system can be given by the following equation:

$$\begin{cases} S_+ = \left(\sqrt{\frac{1}{b}}, 0, 0, \gamma\right), \\ S_0 = (0,0,0,\gamma), \\ S_- = \left(-\sqrt{\frac{1}{b}}, 0, 0, \gamma\right), \end{cases} \tag{6}$$

where γ is an arbitrary constant, so that system (4) has three-line equilibrium points parallel to the x_4-axis. For the Jacobi matrix at the equilibrium points can be expressed as

$$J_s = \begin{bmatrix} 0 & 1-\gamma^2 & 0 & 0 \\ 0 & 0 & 1 & 0 \\ 1-3bx^2 & -a & -1 & 0 \\ 0 & 1 & 0 & 0 \end{bmatrix}. \tag{7}$$

For S_0, the characteristic equation of Eq. (7) can be expressed as

$$\lambda\left[\lambda^3 + \lambda^2 + a\lambda + \gamma^2 - 1\right] = 0. \tag{8}$$

For S_+ and S_-, the characteristic equation of Eq. (7) can be expressed as

$$\lambda\left[\lambda^3 + \lambda^2 + a\lambda + 2(1-\gamma^2)\right] = 0. \tag{9}$$

It can be found that the position of the trilinear equilibrium point is determined by the system parameter b and the initial condition $x_4(0)$ of the memristor, while its stability is determined by the system parameter a and the initial condition $x_4(0)$ of the memristor.

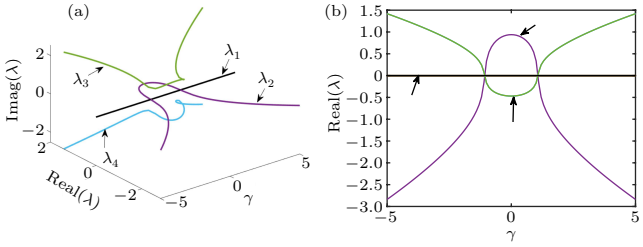


Fig. 6. For S_0, the distribution of eigenvalues about γ. (a) Real, imaginary parts of the eigenvalues on γ, (b) real parts of the eigenvalues on γ.

The eigenvalue curves for S_0 are shown in Fig. 6, where λ_1 and λ_2 are real eigenvalues, λ_3 and λ_4 are a pair of complex conjugate eigenvalues, and it can be seen from the Fig. 6 that for $\gamma < -1.073$ and $\gamma > 1.073$, S_0 is a saddle focus for indicator 2; for $-1.073 < \gamma < 1.073$, S_0 is a saddle focus for indicator 1. The eigenvalue curves for S_+ and S_- are shown in Fig. 7. Similarly, for $\gamma < -0.961$ and $\gamma > 0.961$, $S_\pm$ is the saddle focus of both indicators 1; for $-0.961 < \gamma$ and $\gamma > 0.961$, $S_\pm$ is the saddle focus of both indicators 2.

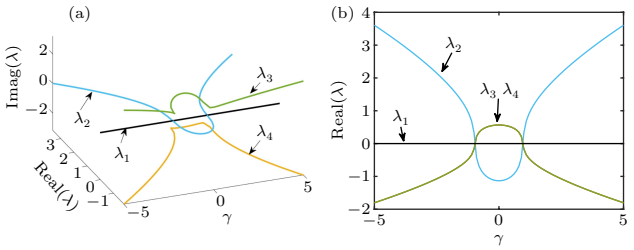


Fig. 7. For S_+ and S_-, the distribution of eigenvalues about S_0. (a) Real, imaginary parts of the eigenvalues on γ, (b) real parts of the eigenvalues on γ.

3. Dimensionality reduction modeling through the MMSVII method

System (4) can easily be implemented using resistors, capacitors, multipliers, and operational amplifiers, but it is difficult to set up the initial conditions of the system in a hardware circuit with strict accuracy. To address this issue, we adopt the MSVII method to reduce the dimensionality of the proposed four-dimensional memristive hyperchaotic jerk system. This results in a three-dimensional reduced model that maps the initial state of the original system to its parameters. The reduced model can effectively analyze the dynamical behavior mechanism and control related to the initial values of the original system, making it easier to capture the extreme multistability phenomenon related to initial values in hardware circuits.

3.1. Incremental integral transformations of state variables

Denoting

$$X_i(t) = \int_0^t x(i)\,\mathrm{d}\tau, \quad \sigma_i = x_i(0), \quad (i = 1,2,3,4). \tag{10}$$

Integrating system (4) from 0 to t,

$$\begin{cases} x_1(t) - x_1(0) = X_2(t) - \int_0^t x_4^2(\tau)x_2(\tau)\,\mathrm{d}\tau, \\ x_2(t) - x_2(0) = X_3(t) + \int_0^t x_3^3(\tau)\,\mathrm{d}\tau, \\ x_3(t) - x_3(0) = X_1(t) - aX_2(t) - X_3(t) \\ \qquad\qquad - b\int_0^t x_1^3(\tau)\,\mathrm{d}\tau - \int_0^t x_3^3(\tau)\,\mathrm{d}\tau, \\ x_4(t) - x_4(0) = X_2(t). \end{cases} \tag{11}$$

From system (4), it is known that $\dot{x}_4 = x_2$, so that $\int_0^t x_4^2(\tau)x_2(\tau)\,\mathrm{d}\tau$ in system (11) can be expressed as

$$\int_0^t x_4^2(\tau)x_2(\tau)\,\mathrm{d}\tau = \int_0^t x_4^2(\tau)\,\mathrm{d}\left[x_4(\tau)\right] = \frac{1}{3}\left[x_4^3(t) - x_4^3(0)\right]. \tag{12}$$

Integrating both sides of $\dot{x}_4 = x_2$ simultaneously from 0 to t gives

$$x_4(t) - x_4(0) = \int_0^t x_2(\tau)\,\mathrm{d}\tau = X_2(t). \tag{13}$$

The difference of squares formula is then used and simplified to give

$$\begin{aligned}&\frac{1}{3}\left[x_4^3(t)-x_4^3(0)\right]\\=&\frac{1}{3}\left[x_4(t)-x_4(0)\right]\cdot\left\{\left[x_4(t)-x_4(0)\right]^2+3x_4(t)\cdot x_4(0)\right\}\\=&\frac{1}{3}X_2\cdot\left[X_2^2+3\cdot\frac{(X_2+2\sigma_4)^2-X_2^2}{4}\right]\\=&\frac{1}{3}X_2^3+\sigma_4X_2(X_2+\sigma_4).\end{aligned}\tag{14}$$

Substituting into Eq. (11) gives

$$\begin{cases}\dot{X}_1=X_2-\frac{1}{3}X_2^3-\sigma_4X_2(X_2+\sigma_4)+\sigma_1,\\ \dot{X}_2=X_3+\int_0^t x_3^3(\tau)\,\mathrm{d}\tau+\sigma_2,\\ \dot{X}_3=X_1-aX_2-X_3-b\int_0^t x_1^3(\tau)\,\mathrm{d}\tau-\int_0^t x_3^3(\tau)\,\mathrm{d}\tau+\sigma_3,\\ \dot{X}_4=X_2+\sigma_4.\end{cases}\tag{15}$$

Clearly the fourth equation in system (15) is independent of the other three equations, so system (15) can be simplified to

$$\begin{cases}\dot{X}_1=X_2-\frac{1}{3}X_2^3-\sigma_4X_2(X_2+\sigma_4)+\sigma_1,\\ \dot{X}_2=X_3+\int_0^t x_3^3(\tau)\,\mathrm{d}\tau+\sigma_2,\\ \dot{X}_3=X_1-aX_2-X_3-b\int_0^t x_1^3(\tau)\,\mathrm{d}\tau-\int_0^t x_3^3(\tau)\,\mathrm{d}\tau+\sigma_3.\end{cases}\tag{16}$$

As the special intrinsic structure relation of the memristor, the higher-order integral terms associated with the memristor can be represented by the state variables of the new mapping, whereas for the higher-order terms of the second and third equations, it is difficult to represent them. To solve this problem, new state variables can be defined as

$$\begin{cases}W=\int_0^t x_3^3(\tau)\,\mathrm{d}\tau,\\ V=b\int_0^t x_1^3(\tau)\,\mathrm{d}\tau.\end{cases}\tag{17}$$

Adding Eq. (17) to system (16) yields a new system of

$$\begin{cases}\dot{X}_1=X_2-\frac{1}{3}X_2^3-\sigma_4X_2(X_2+\sigma_4)+\sigma_1,\\ \dot{X}_2=X_3+W+\sigma_2,\\ \dot{X}_3=X_1-aX_2-X_3-V-W+\sigma_3,\\ \dot{W}=(X_1-aX_2-X_3-V-W+\sigma_3)^3,\\ \dot{V}=b\left\{X_2-\frac{1}{3}X_2^3-\sigma_4X_2(X_2+\sigma_4)+\sigma_1\right\}^3.\end{cases}\tag{18}$$

From Eq. (10), the initial value of system (18) is 0. However, when $\sigma_2=10^{-6}$, $\sigma_1=\sigma_3=\sigma_4=0$, the trajectory of system (18) gradually begins to expand, as shown in Fig. 8.

3.2. Linear transformation of state variables

Looking at Fig. 8, one can see that the system diverges to some extent in all planes, and a synthesis of Ref. [13], together with the characteristics of the three equations of the system, allows for the introduction of three new state variables as

$$\begin{cases}Y_1=2(X_1-V),\\ Y_2=X_2,\\ Y_3=2(X_3+W).\end{cases}\tag{19}$$

Deriving Eq. (19) and substituting it into Eq. (18) gives

$$\begin{cases}\dot{Y}_1=2\left\{Y_2-\frac{1}{3}Y_2^3-\sigma_4Y_2(Y_2+\sigma_4)+\sigma_1\right.\\ \qquad\left.-b\left[Y_2-\frac{1}{3}Y_2^3-\sigma_4Y_2(Y_2+\sigma_4)+\sigma_1\right]^3\right\},\\ \dot{Y}_2=0.5Y_3+\sigma_2,\\ \dot{Y}_3=2\Big[0.5Y_1-0.5Y_3-aY_2+\sigma_3\\ \qquad+(0.5Y_1-0.5Y_3-aY_2+\sigma_3)^3\Big].\end{cases}\tag{20}$$

Since the initial values $X_1(0)$, $X_2(0)$, $X_3(0)$, and $W(0)$ of the system (18) are both 0, the initial values $Y_1(0)$, $Y_2(0)$, and $Y_3(0)$ of the system (20) are also fixed to 0. When the parameters of system (20) are set to be the same as those of system (18), the phase diagram of the system is shown in Fig. 9. It is clear that the method of dimensionality reduction modeling of the system proposed in this paper can effectively eliminate divergence.

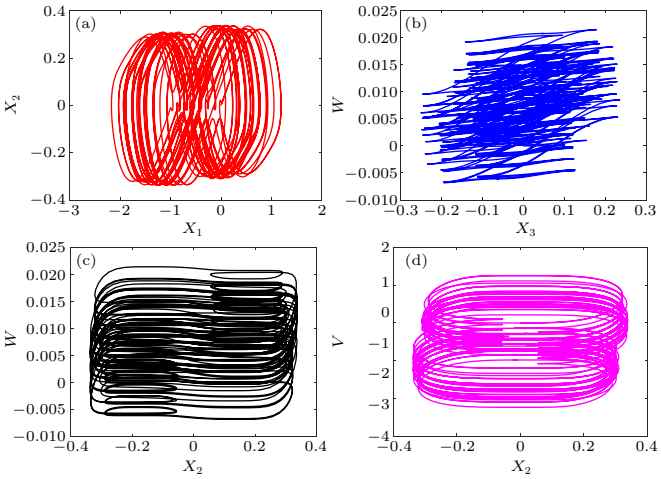


Fig. 8. Phase diagram of system (18) when $a=0.68$, $b=20$, $\sigma_2=10^{-6}$, and $\sigma_1=\sigma_3=\sigma_4=0$. (a) X_1–X_2 plane, (b) X_1–W plane, (c) X_2–W plane, (d) X_2–V plane.

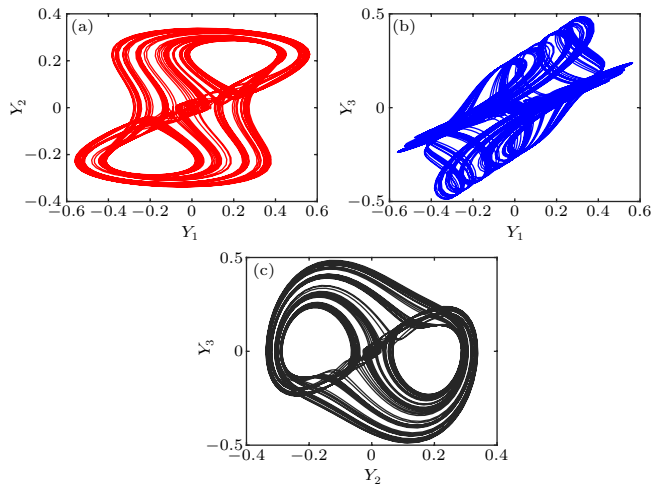


Fig. 9. Phase diagram of system (20) when $a=0.68$, $b=20$, $\sigma_2=10^{-6}$, and $\sigma_1=\sigma_3=\sigma_4=0$. (a) Y_1–Y_2 plane, (b) Y_1–Y_3 plane, (c) Y_2–Y_3 plane.

Comparing system (20) with system (4), it can be found that the final system obtained is related to the initial system (4)

as

$$\begin{cases} x_1(t) = \dot{X}_1 = Y_2 - \frac{1}{3}Y_2^3 - \sigma_4 Y_2(Y_2+\sigma_4) + \sigma_1, \\ x_2(t) = \dot{X}_2 = 0.5Y_3 + \sigma_2, \\ x_3(t) = \dot{X}_3 = 0.5Y_1 - 0.5Y_3 - aY_2 + \sigma_3, \\ x_4(t) = \dot{X}_4 = Y_2 + \sigma_4. \end{cases} \tag{21}$$

Let $Z_1 = x_1(t)$, $Z_2 = x_2(t)$, $Z_3 = x_3(t)$, and $Z_4 = x_4(t)$. The phase diagrams drawn from the relations described in Eq. (21) are shown in Fig. 10; it can be noticed that they show the same topology as the initial system (4).

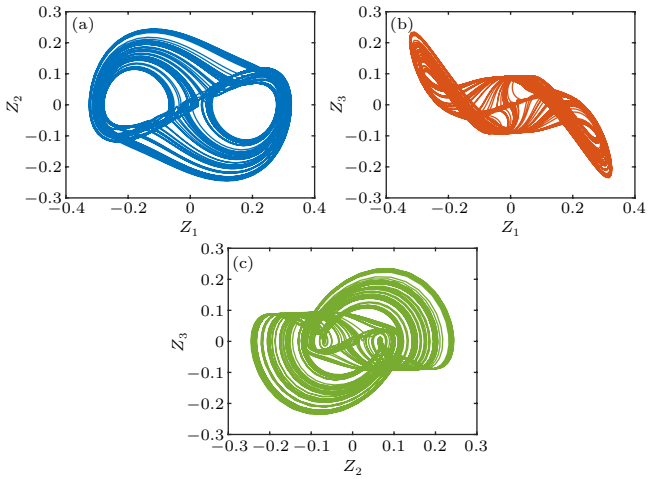


Fig. 10. Phase diagram of system (21) when $a = 0.68$, $b = 20$, $\sigma_2 = 10^{-6}$, and $\sigma_1 = \sigma_3 = \sigma_4 = 0$. (a) Z_1–Z_2 plane, (b) Z_1–Z_3 plane, (c) Z_2–Z_3 plane.

3.3. Switching equilibrium points and stabilities

Let $\dot{Y}_1 = \dot{Y}_2 = \dot{Y}_3 = 0$,

$$\begin{cases} 0 = 2\Big\{Y_2 - \frac{1}{3}Y_2^3 - \sigma_4 Y_2(Y_2+\sigma_4) + \sigma_1 \\ \quad - b\left[Y_2 - \frac{1}{3}Y_2^3 - \sigma_4 Y_2(Y_2+\sigma_4) + \sigma_1\right]^3\Big\}, \\ 0 = 0.5Y_3 + \sigma_2, \\ 0 = 2\Big[0.5Y_1 - 0.5Y_3 - aY_2 + \sigma_3 \\ \quad + (0.5Y_1 - 0.5Y_3 - aY_2 + \sigma_3)^3\Big]. \end{cases} \tag{22}$$

Clearly, the equilibrium point of the system (20) can be expressed as $E = (2(a\mu - \sigma_2 - \sigma_3), \mu, -2\sigma_2)$, when the parameters satisfy

$$\mu - \frac{1}{3}\mu^2 - (\mu+\sigma_4)\sigma_4\mu + \sigma_1 = 0 \ \text{ or}$$
$$\mu - \frac{1}{3}\mu^2 - (\mu+\sigma_4)\sigma_4\mu + \sigma_1 = \pm\sqrt{\frac{1}{b}}. \tag{23}$$

Conversely, when $b \le 0$, μ satisfies

$$\mu - \frac{1}{3}\mu^2 - (\mu+\sigma_4)\sigma_4\mu + \sigma_1 = 0. \tag{24}$$

When the parameter σ_4 is a variable and $a = 0.68$, $b = 20$, $\sigma_1 = 0$, $\sigma_2 = 10^{-6}$, $\sigma_3 = 0$, this gives the Jacobian matrix of the system at the equilibrium point

$$J_s = \begin{bmatrix} 0 & K & 0 \\ 0 & 0 & 0.5 \\ 1 & -2a & -1 \end{bmatrix}. \tag{25}$$

By calculation, the characteristic equation can be expressed by the following equation:

$$\lambda^3 + \lambda^2 + a\lambda - 0.5K = 0, \tag{26}$$

where $K = 2\left(-\mu^2 - 2\sigma_4\mu + 1 - \sigma_4^2\right)$ when μ satisfies $\mu - \frac{1}{3}\mu^3 - (\mu+\sigma_4)\sigma_4\mu = 0$, and when μ satisfies $\mu - \frac{1}{3}\mu^3 + (\mu - \sigma_4)\sigma_4\mu = \pm\sqrt{1/b}$, $K = -4(-\mu^2 - 2\sigma_4\mu + 1 - \sigma_4^2)$.

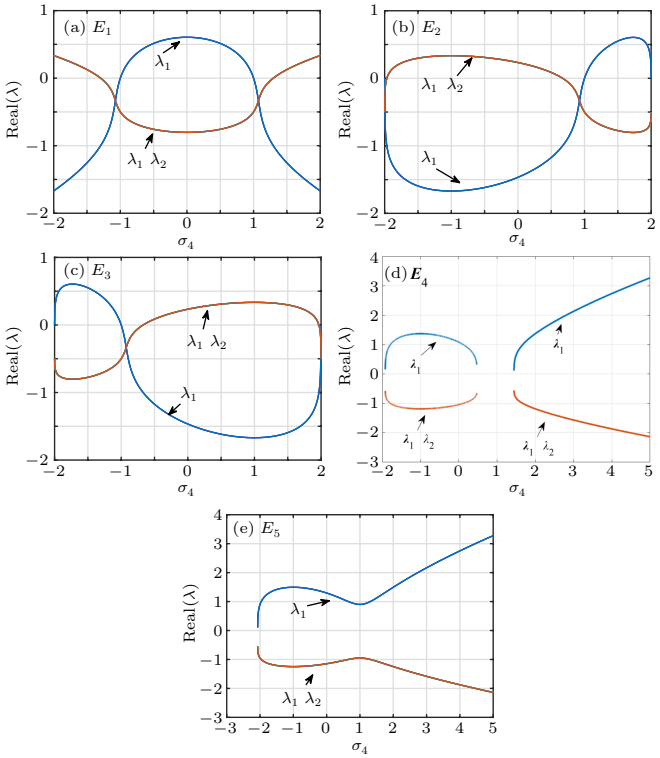


Fig. 11. The equilibrium point is about the position and stability of the parameter σ_4, (a) E_1, (b) E_2, (c) E_3, (d) E_4, (e) E_5.

Table 1. The type of the equilibrium points of parameter σ_4.

Equilibrium points	The range of parameter σ_4	The type of equilibrium points
E_1	$(-\infty,-1.29)\cup(1.29,+\infty)$	index-2 saddle-foci
E_1	$(-1.29,-1)\cup(1,1.29)$	stable saddle-foci
E_1	$(-1,1)$	index-1 saddle-foci
E_2	$(-2,-1.97)\cup(0.671,1)$	stable saddle-foci
E_2	$(-1.97,0.671)$	index-2 saddle-foci
E_2	$(1,2)$	index-1 saddle-foci
E_3	$(-1,-0.671)\cup(1.97,2)$	stable saddle-foci
E_3	$(-2,1)$	index-1 saddle-foci
E_3	$(-0.671,1.97)$	index-2 saddle-foci
E_4	$(-1.921,0.4708)\cup(1.442,+\infty)$	index-1 saddle-foci
E_5	$(-2.071,+\infty)$	index-1 saddle-foci

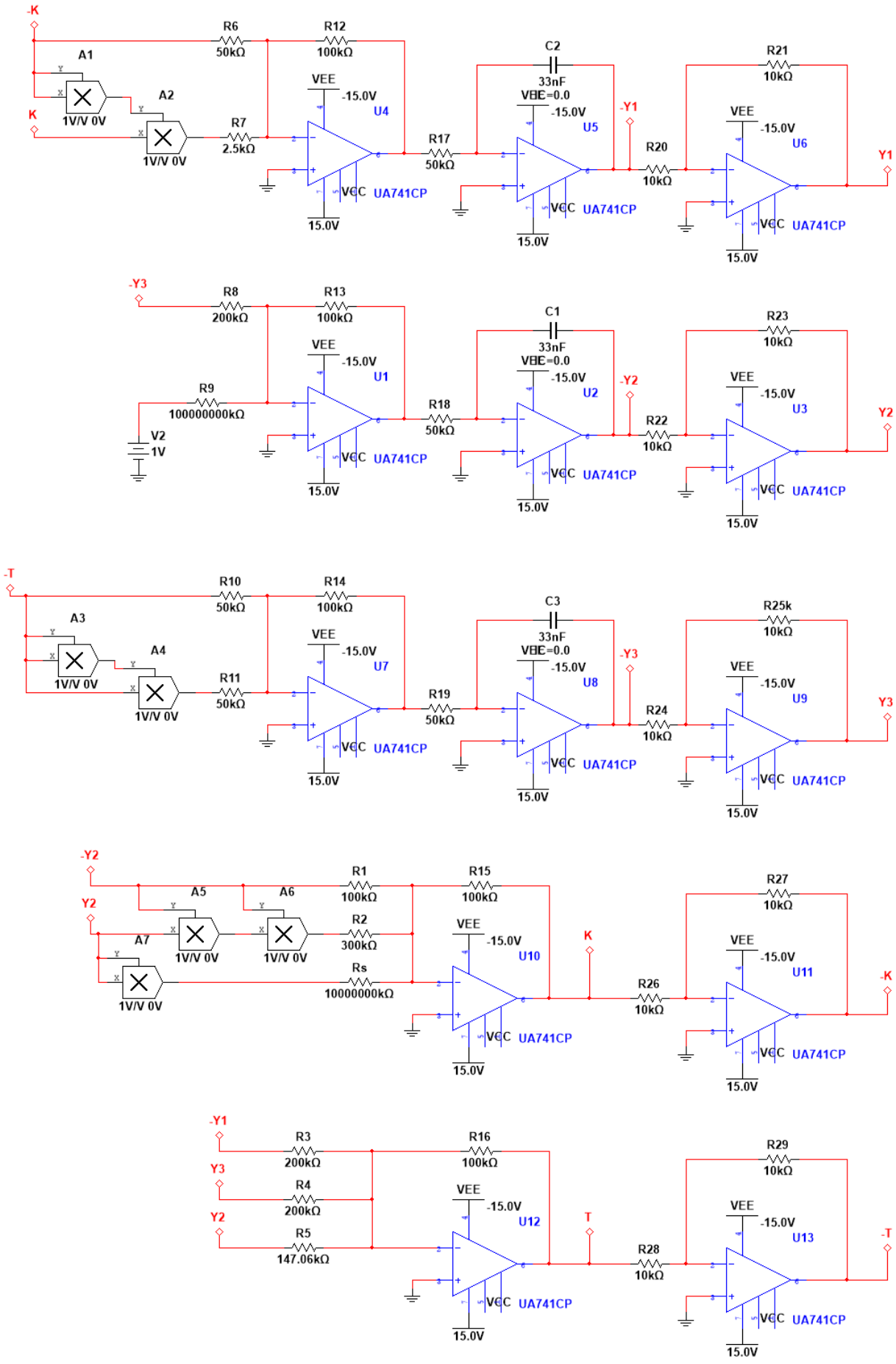


Fig. 12. Multisim simulation circuit diagram for system (20).

When μ satisfies $\mu-\frac{1}{3}\mu^3-(\mu+\sigma_4)\sigma_4\mu=0$, the real number solution to the equation can be expressed as

$$\begin{cases}\mu_1=0,\ \ \mu_2=\frac{-3\sigma_4+\sqrt{12-3\sigma_4^2}}{2},\\ \mu_3=\frac{-3\sigma_4-\sqrt{12-3\sigma_4^2}}{2},\ \ (-2\le\sigma_4\le 2),\\ \mu_1=\mu_2=\mu_3=0,\ \ (\sigma_4\in(-\infty,-2)\cup(2,+\infty)).\end{cases}\tag{27}$$

Therefore, when $-2\le\sigma_4\le 2$, the equilibrium points of the system (20) are

$$\begin{cases}E_1=(0,0,0),\\ E_2=(0.68(-3\sigma_4+\sqrt{12-3\sigma_4^2}),\frac{-3\sigma_4+\sqrt{12-3\sigma_4^2}}{2},0),\\ E_3=(0.68(-3\sigma_4-\sqrt{12-3\sigma_4^2}),\frac{-3\sigma_4-\sqrt{12-3\sigma_4^2}}{2},0).\end{cases}\tag{28}$$

Furthermore, when $\sigma_4<-2$ or $\sigma_4>2$, the equilibrium point of the system (20) is $E_1=(0,0,0)$, their positions and stabilities are shown in Figs. 11(a)–11(c) and Table 1. And when μ satisfies $\mu-\frac{1}{3}\mu^3-(\mu+\sigma_4)\sigma_4\mu=\pm\sqrt{1/b}$, using the Cardano formula, the real number solution to the equation can be expressed as

$$\begin{cases}\mu_4=\sqrt[3]{-\frac{q_1}{2}+\sqrt{\left(\frac{q_1}{2}\right)^2-1}}\\ \qquad+\sqrt[3]{-\frac{q_1}{2}-\sqrt{\left(\frac{q_1}{2}\right)^2-1}}-\sigma_4,\\ \mu_5=\omega^2\sqrt[3]{-\frac{q_2}{2}+\sqrt{\left(\frac{q_2}{2}\right)^2-1}}\\ \qquad+\omega\sqrt[3]{-\frac{q_2}{2}-\sqrt{\left(\frac{q_2}{2}\right)^2-1}}-\sigma_4,\end{cases}\tag{29}$$

where $q_1=-\sigma_4^3+3\sigma_4+3\sqrt{1/b}$ and $q_2=-\sigma_4^3+3\sigma_4-3\sqrt{1/b}$.

Therefore, the equilibrium points of the system at $\mu-\frac{1}{3}\mu^3+(\mu-\sigma_4)\sigma_4\mu=\pm\sqrt{1/b}$ can be expressed as $E_i=(2(a\mu_i-\sigma_2-\sigma_3),\mu_i,-2\sigma_2)$, where $i=4,5$. Through calculation, it can be found that when $\sigma_4\in(-1.921,0.4708)\cup(1.442,+\infty)$, μ_4 is a constant solution, and when $\sigma_4\in(-2.071,+\infty)$, μ_5 is a constant solution. The position and stabilities of the equilibrium points E_4 and E_5 are shown in Figs. 11(d)–11(e) and Table 1.

4. Multisim digital circuit implementation

To verify the results of the MATLAB numerical simulation, a Multisim equivalent circuit for system (20) was constructed, based on Eq. (20) and the basic operational circuit modules (summation, integration, inverse, etc.), using an equivalent circuit model designed with components such as resistors, capacitors, operational amplifiers, and analog multipliers. Through Kirchhoff's laws, we can obtain the circuit equations of the system (20) can be expressed as

$$\begin{cases}R_0C_0Y_1=\frac{R}{R_6}\left(\frac{R}{R_1}Y_2-\frac{R}{R_2}Y_2^3-\frac{R}{R_S}Y_2^2\right)\\ \qquad-\frac{R}{R_7}\left(\frac{R}{R_1}Y_2-\frac{R}{R_2}Y_2^3-\frac{R}{R_S}Y_2^2\right)^3,\\ R_0C_0Y_2=\frac{R}{R_8}Y_3+\frac{R}{R_9},\\ R_0C_0Y_3=\frac{R}{R_{10}}\left(\frac{R}{R_3}Y_1-\frac{R}{R_4}Y_3-\frac{R}{R_5}Y_{22}\right)\\ \qquad+\frac{R}{R_{11}}\left(\frac{R}{R_3}Y_1-\frac{R}{R_4}Y_3-\frac{R}{R_5}Y_{22}\right)^3,\end{cases}\tag{30}$$

where $\frac{R}{R_6}=2$, $\frac{R}{R_1}=1-\sigma_4^2$, $\frac{R}{R_2}=\frac{1}{3}$, $\frac{R}{R_S}=\sigma_4$, $\frac{R}{R_7}=2b$, $\frac{R}{R_8}=0.5$, $\frac{R}{R_9}=\sigma_2$, $\frac{R}{R_{10}}=2$, $\frac{R}{R_3}=0.5$, $\frac{R}{R_4}=0.5$, $\frac{R}{R_5}=a$, $\frac{R}{R_{11}}=2$, $C_1=C_2=C_3=33$ nF, $R_{12}=R_{13}=R_{14}=R_{15}=R_{16}=100$ kΩ, $R_{17}=R_{18}=R_{19}=50$ kΩ, $R_{20}=R_{21}=R_{22}=R_{23}=R_{24}=R_{25}=R_{26}=R_{27}=R_{28}=R_{29}=10$ kΩ. So we can obtain $R_S=\frac{R}{\sigma_4}$, $R_1=\frac{100}{1-\sigma_4^2}$ kΩ, $R_2=300$ kΩ, $R_3=200$ kΩ, $R_4=200$ kΩ, $R_5=\frac{100}{a}$ kΩ, $R_6=50$ kΩ, $R_7=\frac{100}{2b}$ kΩ, $R_8=200$ kΩ, $R_9=\frac{100}{\sigma_2}$ kΩ, $R_{10}=50$ kΩ and $R_{11}=50$ kΩ.

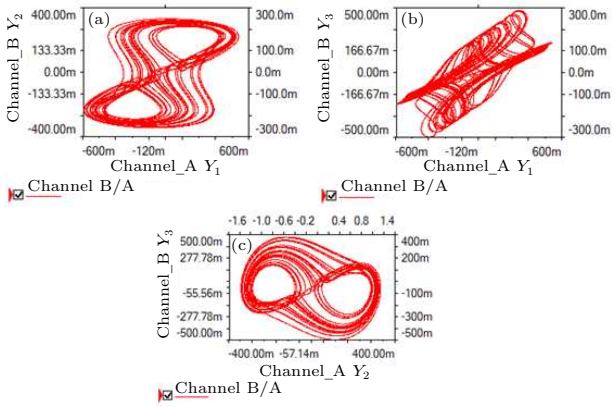


Fig. 13. Multisim simulation results for system (20). (a) Y_1–Y_2 plane, (b) Y_1–Y_3 plane, (c) Y_2–Y_3 plane.

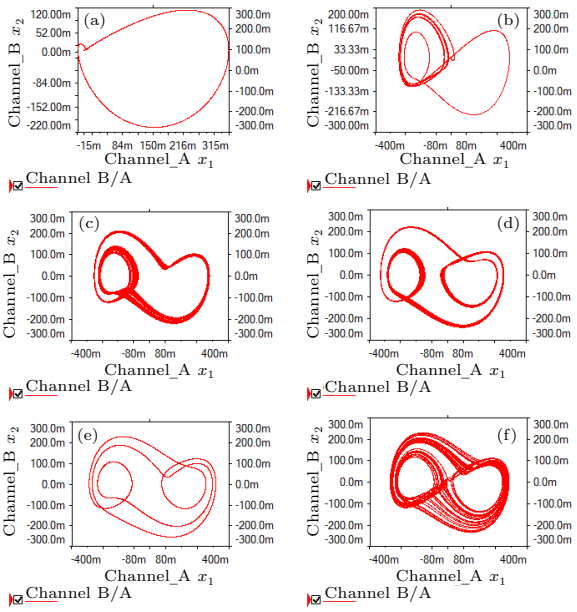


Fig. 14. Simulation results for various attractors generated by the system (20) with different values of σ_4: (a) $x_4(0)=-0.7$, (b) $x_4(0)=-0.31$, (c) $x_4(0)=-0.27$, (d) $x_4(0)=-0.23$, (e) $x_4(0)=-0.16$, (f) $x_4(0)=-0.14$.

The circuit diagram and simulation results for system (20) are shown in Figs. 12 and 13. In addition, the phase diagram of the system (20) was also numerically simulated for different values of σ_4, as shown in Figs. 14(a)–14(f).

5. Conclusion

In this paper, a four-dimensional memristive hyperchaotic jerk system is obtained by adding an ideal memristor to the jerk chaotic system. This four-dimensional memristive hyperchaotic jerk system has three equilibrium points controlled by the system parameters b and the initial condition $x_4(0)$. Thus, with the system parameters a and b held constant, the system generates multiple coexisting attractors as the initial value of the memristor changes, resulting in an extreme multistability phenomenon.

To explain the control mechanism of extreme multistability phenomena from within, this paper uses a method consisting of incremental integral transformations of state variables and linear transformations to reconstruct and model this memristive jerk system, successfully constructing a three-dimensional reduced-dimension system that maintains the dynamics of the original four-dimensional system. A phase diagram based on the relationship between the primitive system and the reduced-dimension system then reveals that the method can be very effective in solving the divergence problem arising from the newly mapped state variables. Finally, based on this reduced-dimension model, extreme multistability phenomena with a large number of coexisting attractors are explained by analyzing the deterministic equilibrium points of the system. In addition, Multisim simulated circuit simulations of the reduced-dimension system are carried out, and the simulation results are in agreement with the MATLAB numerical simulation results.

Acknowledgments

Project supported by the National Natural Science Foundation of China (Grant No. 62071411) and the Research Foundation of Education Department of Hunan Province, China (Grant No. 20B567).

References

[1] Ott E, Grebogi C and Yorke J A 1990 *Controlling Chaos* **64** 1196
[2] Lü J, Chen G and Cheng D 2004 *Int. J. Bifurcat. Chaos* **14** 1507
[3] Chlouverakis K E and Sprott J C 2006 *Chaos Solitons & Fractals* **28** 739
[4] Tigan G and Opriş D 2008 *Chaos Solitons & Fractals* **36** 1315
[5] Pham V T, Jafari S and Wang X 2016 *Int. J. Bifurcat. Chaos* **26** 1650069
[6] Li Z, Zhou H and Wang M 2021 *Nonlinear Dyn.* **104** 1455
[7] Ma M, Yang Y and Qiu Z 2022 *Nonlinear Dyn.* **107** 2935
[8] Guo M, Zhu Y and Liu R 2022 *Neurocomputing* **472** 12
[9] Yu F, Shen H, Zhang Z, Huang Y, Cai S and Du S 2021 *Integration* **81** 71
[10] Ma M, Xie X, Yang Y, Li Z and Sun Y 2023 *Chin. Phys. B.* **32** 058701
[11] Wang M, An M and Zhang X 2023 *Nonlinear Dyn.* **111** 1871
[12] Yu F, Xu S and Xiao X 2023 *Integration* **90** 58
[13] Yu F, Zhang W and Xiao X 2023 *Mathematics* **11** 701
[14] Zhou Y, Hua Z and Pun C M 2014 *IEEE Trans. Cybernetics* **45** 2001
[15] Parvaz R and Zarebnia M 2018 *Opt. Laser Technol.* **101** 30
[16] Min F, Cheng Y and Lu L 2021 *Int. J. Bifurcat. Chaos* **31** 2150167
[17] Chen B, Xu Q and Chen M 2021 *Frontiers Inform. Technol. Electron. Eng.* **22** 1517
[18] Chen M, Sun M and Bao H 2019 *IEEE Trans. Ind. Electron.* **67** 2197
[19] Nganso E N, Mbouna S G N and Yamapi R 2023 *Chaos Solitons & Fractals* **169** 113235
[20] Ruiz-Silva A, Gilardi-Velázquez H E and Campos E 2021 *Chaos Solitons & Fractals* **151** 111263
[21] Chen M, Ren X and Wu H 2020 *Chaos Solitons & Fractals* **131** 109544
[22] Chen M, Wang C and Bao H 2020 *Chaos Solitons & Fractals* **140** 110188
[23] Liu T, Yan H and Banerjee S 2021 *Chaos Solitons & Fractals* **145** 110791
[24] Chang H, Li Y and Chen G 2020 *Int. J. Bifurcat. Chaos* **30** 2030019
[25] Lin H, Wang C and Hong Q 2020 *IEEE Transactions on Circuits and Systems II: Express Briefs* **67** 3472
[26] Chen M, Sun M and Bao B 2018 *Nonlinear Dyn.* **91** 1395
[27] Chen M, Feng Y and Bao H 2018 *Chaos Solitons & Fractals* **115** 313
[28] Chen M, Feng Y and Bao H 2019 *Complexity* **140** 110188
[29] Pham V T, Jafari S and Volos C 2019 *Chaos Solitons & Fractals* **120** 213
[30] Idrisi M J and Ullah M S 2021 *New Astronomy* **89** 101629
[31] Kalantonis V S, Vincent A E and Gyegwe J M 2021 *Nonlinear Analysis and Global Optimization* **167** 251
[32] Wang L, Zhang S and Zeng Y C 2018 *Electron. Lett.* **54** 808
[33] Corinto F and Forti M 2017 *IEEE Transactions on Circuits and Systems I: Regular Papers.* **64** 1540
[34] Corinto F and Forti M 2016 *IEEE Transactions on Circuits and Systems I: Regular Papers.* **63** 1997
[35] Itoh M and Chua L O 2013 *Int. J. Bifurcat. Chaos* **23** 1330001
[36] Kengne J, Njitacke Z T and Fotsin H B 2016 *Nonlinear Dyn.* **83** 751
[37] Korneev I A and Semenov V V 2017 *Chaos* **27** 081104